J. Fluid Mech. (1981), *vol*, 109 *pp.* 189–216
Printed in Great Britain

The evolution of an elliptic vortex ring

By M. R. DHANAK
Department of Mathematics, Imperial College, London
AND B. DE BERNARDINIS†
Facoltà di Ingegneria Università di Genova

(Received 28 August 1980)

The evolution of a vortex ring in an ideal fluid under self-induction from a flat and elliptic configuration is followed numerically using the cut-off approximation (Crow 1970) for the velocity at the vortex. Calculations are presented for four different axes ratios of the initial ellipse. A particular choice is made for the core size and vorticity distribution in the core of the vortex ring. When the initial axes ratio is close to 1, the vortex ring oscillates periodically. The periodicity is lost as more eccentric cases are considered. For initial axes ratio 0·2, the calculations suggest a break-up of the ring through the core at one portion of the ring touching that at another, initially distant, portion of the ring.

Results from quantitative experiments, conducted at moderate Reynolds number with the vortex rings produced by puffing air through elliptic orifices, are compared with the calculations. The agreement is fairly good and it is found that a vortex ring produced from an orifice of axes ratio 0·2 breaks up into two smaller rings. The relevance of the results to the vortex trail of an aircraft is discussed.

1. Introduction

In recent years considerable interest has been shown in the mechanism responsible for destroying the trailing vortex system of an aircraft. The trailing vortices, made visible by the condensation of moisture in their cores, are observed to undergo a slow instability: wavy disturbances grow on both trailing vortices and reach an amplitude such that the vortices touch at the nearer points and break up into a sequence of distinct vortex rings. The form of the rings is such that its projection onto the plane of maximum projected area is roughly elliptic in shape. Once the rings have formed, the vortex trail soon ceases to be visible.

The growth of waves on trailing vortices was studied analytically by Crow (1970) who showed that small perturbations of the vortices in the form of plane waves of sufficiently long wavelengths are unstable. Later Moore (1972) followed the growth of symmetrical waves on trailing vortices numerically and showed that waves grow to such an amplitude that they touch at the nearer points. Thus an explanation of the observed looping process is to hand.

The mechanism by which the vortices break up to form vortex rings is not understood. Nor is it clear that the rapid loss of visibility of the rings imply their

† Visiting Physiological Flow Studies Unit, Department of Aeronautics, Imperial College, London, during the preparation of this paper.

disintegration; care must be taken in interpreting observations which depend on the retention of smoke particles or water droplets in the vortex cores. It is possible that the non-circular form of the vortex rings which are formed is significant to the observations. Thus it is of interest to know what happens to an initially non-circular vortex ring.

In this paper an initial-value problem is studied. Given a plane elliptic vortex ring, it is proposed to follow its subsequent motion and deformation numerically. It will be shown below that a non-circular ring must necessarily deform.

The choice of a vortex ring of elliptic shape is also relevant to the study of a wake of a bird in forward flight. Photographs from Kokshaysky's (1979) experiments clearly show deforming vortex rings in the wake. The motion of the wings is such that in one complete beat the bird leaves behind it a vortex ring of roughly elliptic shape in a plane inclined at an angle to the direction of flight. Rayner (1979) has modelled such a wake by a chain of elliptic vortex rings to estimate power consumption and mean lift coefficients. He ignores the deformation of the rings in his calculations.

Previous numerical study of the motion of an elliptic vortex ring is due to Arms & Hama (1965) (see also Viets & Sforza 1975) who used local induction approximation in their calculation of the motion. This assumes that the motion of a thin vortex filament is governed by the approximate equations

$$\frac{\partial \mathbf{X}(s,t)}{\partial t^*} = \frac{\mathbf{b}(s,t)}{\rho(s,t)}, \quad t^* = \frac{\Gamma}{4\pi} \ln(1/\epsilon)\, t, \tag{1.1}$$

where $\mathbf{b}$ and ρ are respectively the local binormal and radius of curvature at $\mathbf{X}$, a point on the filament, and s is the arc distance along the filament. ϵ is taken to be an unspecified constant although a proper treatment of the Biot–Savart integral shows that $\epsilon = c/\rho$, where c is the core radius. Thus the approximation neglects the dependence of ϵ on ρ and on any variations of the core size during the motion as well as neglecting the contribution to velocity from distant parts of the vortex. The neglecting of this contribution means that the approximation loses the Crow instability. Thus the approximation is not satisfactory if this important feature of the evolution of a vortex filament is not to be excluded from consideration.

The cut-off theory, due to Crow (1970), provides a more accurate method of approach and is used here to study the motion of the vortex ring. The fluid is regarded as inviscid, incompressible and of uniform density. Wherever possible, the vortex ring is treated as being of zero cross-section and the velocity field due to the vortex is calculated using the Biot–Savart line integral. Then Helmholtz law, that in inviscid fluid vortex lines move with the fluid, leads to an integro-differential equation for the motion of the vortex ring.

However, the Biot–Savart line integral diverges on the vortex ring itself. The difficulty is overcome by means of a 'cut-off', the choice of which depends on the structure of the vortex ring. The influence of the internal structure on the motion of the vortex ring enters only through the cut-off.

A rigorous justification of the cut-off method for finite-amplitude disturbances to a vortex has been provided by Moore & Saffman (1972).† In the absence of axial flow in the vortex filament, which is the case here, they show that the error in the velocity obtained by the cut-off method is $O(c^2/\rho^2)$. The method is described more fully later.

† The earlier justification of Widnall, Bliss & Zalay (1971) does not specify how the cross-sectional area of the vortex filament is to vary; the variation is negligible for infinitesimal distortions of the vortex, but it cannot be ignored for finite-amplitude distortions.

It may be noted from (1.1) that the velocity at a point on the vortex is approximately inversely proportional to the local radius of curvature. Since the curvature varies along the length of an elliptic vortex ring, the velocity will vary accordingly so that the ring will deform from its elliptic shape as it moves. Experiments by Oshima (1972) with vortex rings of initially lenticular shape and by Kambe & Takao (1971) with various other non-circular initial shapes qualitatively show the deformation of such vortex rings.

In §2, small perturbations of elliptic mode to a circular vortex ring are discussed while in §3 the numerical procedure used to integrate the equation of motion of an initially elliptic vortex ring is described. In §4 numerical results are presented for vortex rings of different eccentricity and core size. The initial core size used for each elliptic ring is that predicted by considering the impulsive motion, in a perfect fluid, of a flat elliptic disc which is then dissolved away. This method of fixing the core size is due to Taylor (1953) and is described in appendix A.

In §5, a quantitative experiment is described for observing the motion of an initially elliptic vortex ring produced by puffing air through an elliptic orifice. The results of the experiment are compared with those of the numerical calculations in §6. Estimates of the vortex parameters for rings produced in this way are obtained in appendix B using a simple model (Saffman 1978) of the flow.

In §7 the relevance of the results to the vortex trail of an aircraft is discussed.

2. Linear theory

The stability of a thin circular vortex ring to small sinusoidal perturbations was considered by Widnall & Sullivan (1973). In a co-ordinate system moving with the velocity of an unperturbed circular vortex ring V, the perturbed ring was taken to be

$$\mathbf{X} = (R + re^{im\theta})\,\mathbf{e}_r + ze^{im\theta}\,\mathbf{e}_z \tag{2.1}$$

where $\mathbf{e}_r$ and $\mathbf{e}_z$ are unit vectors in the radial and axial directions, θ is the azimuthal angle, R is the radius of the unperturbed ring and $|r|, |z| \ll R$. The wavenumber m is an integer.

On substituting (2.1) into the equation of motion (3.1) and linearizing in z and r, it was shown that for moderate values of m (for which it is valid to use (3.1)), for each m the ring oscillates with an angular frequency $\pm\alpha_m$ (see Widnall & Sullivan 1973).

In the case $m = 2$, the two solutions corresponding to $\pm\alpha_2$ can be superposed to satisfy the condition that initially the perturbed vortex ring has a plane elliptic form. This gives

$$r(t) = r_0 \cos(\alpha_2 t), \quad z(t) = z_0 \sin(\alpha_2 t) \tag{2.2}$$

where r_0 and z_0 are real constants.

Using the value of α_2 as given by Widnall & Sullivan, it follows that the period of oscillations $2\pi/\alpha_2$, which depends on R and the internal structure of the vortex (i.e. core radius and vorticity distribution), is given by

$$\tau(R, c, A) = \frac{8\pi^2 R^2}{\Gamma}\left[\{4(\ln c/R - A) + 0{\cdot}22\}\{3(\ln c/R - A) + 2{\cdot}23\}\right]^{-\frac{1}{2}}, \tag{2.3}$$

where c is the core radius and

$$A = \frac{4\pi^2}{\Gamma^2}\int_0^c rv^2\,dr. \tag{2.4}$$

Here v is the swirl velocity in the core and there is no axial flow in the filament. Note that in linearized stability theory the length of the vortex filament remains constant so that c must also be a constant (see § 3 below).

The self-induced mean velocity of the ring is that of the unperturbed circular ring,

$$\mathbf{V}(R, c, A) = \frac{\mathbf{e}_z \Gamma}{4\pi R}\left(\ln\frac{8R}{c} + A - \tfrac{1}{2}\right). \tag{2.5}$$

3. The equation of motion and the procedure for numerical integration

Suppose that in a co-ordinate system fixed with respect to flow at infinity the centre-line of the vortex ring at time t occupies the curve given parametrically by $\mathbf{X}(\xi, t)$ where ξ is chosen so that $\xi =$ constant always refers to the same fluid particle. Then, if the vortex ring has circulation Γ, its motion is governed by

$$\frac{\partial \mathbf{X}}{\partial t}(\xi_0, t) = \frac{\Gamma}{4\pi}\oint \frac{\partial \mathbf{X}}{\partial \xi}(\xi, t) \wedge \frac{(\mathbf{X}(\xi_0, t) - \mathbf{X}(\xi, t))}{|\mathbf{X}(\xi_0, t) - \mathbf{X}(\xi, t)|^3}\, d\xi \tag{3.1}$$

where $\oint$ implies that a suitable cut-off is used to make the integral finite at $\xi = \xi_0$.

Following Moore (1972), the method of cut-off chosen here is that due to Rosenhead. Thus in (3.1) the denominator in the integrand is replaced by $\{|\mathbf{X}(\xi_0, t) - \mathbf{X}(\xi, t)|^2 + \mu^2\}^{\frac{3}{2}}$ where μ is proportional to $c(\xi_0, t)$, the local radius of the core (assumed to be circular). Thus $\mu = 2\delta_R c$ where δ_R is determined by evaluating the velocity of a circular vortex ring using the cut-off integral and comparing it with the known exact result given by Saffman (1970). Thus

$$\ln 2\delta_R = -\tfrac{1}{2} - A \tag{3.2}$$

where A is given by (2.4). The crucial assumption is that μ is independent of the geometric shape of the vortex filament and depends only on the local structure of the vortex. Thus the same value of δ_R as for a circular vortex ring can be used for a vortex filament of any shape provided their local structures are the same.

Moore & Saffman (1972) show that any variation in the internal structure along the length of the filament are smoothed out in a time which is short compared with the time scale associated with the change in the geometric configuration of the filament. Thus on the time scale of filament motion the core radius c and the swirl velocity v are independent of position along the vortex ring. $c = c(t)$ such that the incompressibility constraint is satisfied so that, if L is the length of the vortex ring, $Lc^2 =$ constant.† Also $v = v(r, t)$, where r is the radial distance from the centre-line of the ring, so that, in view of the conservation of circulation,

$$v = \frac{\Gamma}{2\pi r} f\left(\frac{r}{c}\right), \quad f(1) = 1, \tag{3.3}$$

where f is determined from the initial structure of the vortex. Thus from (2.4)

$$A = \int_0^1 \frac{1}{\eta} f^2(\eta)\, d\eta, \tag{3.4}$$

so that A is a constant throughout the motion, as required.

† Leonard (1974) has considered models where the cut-off length is chosen so that volume of local filament segment is conserved and also where the influence of diffusion of vorticity is incorporated in the cut-off length.

The Lagrangian parameter ξ is chosen so that in a fixed Cartesian co-ordinate system $Oxyz$, the vortex ring is initially given by

$$\mathbf{X}(\xi, 0) = (a\cos\xi, b\sin\xi, 0), \quad -\pi \leqslant \xi \leqslant \pi, \tag{3.5}$$

where a and b are respectively the semi-major and semi-minor axes of the ellipse.

For time $t > 0$, it is assumed that the vortex ring retains its symmetry about $x = 0$ and $y = 0$ so that, writing $\mathbf{X} = (x, y, z)$

$$\left.\begin{aligned} x(-\pi+\xi,t) &= x(\pi-\xi,t) = -x(\xi,t) = -x(-\xi,t),\\ y(-\pi+\xi,t) &= -y(\pi-\xi,t) = -y(\xi,t) = y(-\xi,t),\\ z(-\pi+\xi,t) &= z(\pi-\xi,t) = z(\xi,t) = z(-\xi,t), \end{aligned}\right\} 0 \leqslant \xi \leqslant \tfrac{1}{2}\pi. \tag{3.6}$$

Hence it is only necessary to follow, say, the portion $0 \leqslant \xi < \frac{1}{2}\pi$ of the ring to obtain the shape of the whole ring.

The evolution of the vortex ring can now be determined by simply integrating (3.1) forward in time and calculating the length of the filament at each time step to obtain the value of $\mu(t)$. However, the integrand in the cut-off integral, although it is finite everywhere, is large in the neighbourhood of ξ_0. For near ξ_0 (suppressing the explicit time-dependence for convenience),

$$\frac{\partial\mathbf{X}(\xi)}{\partial\xi} \wedge \frac{\mathbf{X}(\xi_0)-\mathbf{X}(\xi)}{\{|\mathbf{X}(\xi_0)-\mathbf{X}(\xi)|^2+\mu^2\}^{\frac{3}{2}}} \sim \left(\frac{\partial\mathbf{X}}{\partial\xi}\right)_0 \wedge \left(\frac{\partial^2\mathbf{X}}{\partial\xi^2}\right)_0 P(\xi); \tag{3.7}$$

where 0 implies that the quantities are evaluated at ξ_0 and

$$P(\xi) = \frac{\frac{1}{2}(\xi-\xi_0)^2}{\left\{(\xi-\xi_0)^2\left(\frac{\partial\mathbf{X}}{\partial\xi}\right)_0^2+\mu^2\right\}^{\frac{3}{2}}}.$$

This would cause a loss of accuracy in evaluating the integral. To overcome this difficulty, the equation of motion is written as

$$\frac{\partial\mathbf{X}}{\partial t}(\xi_0,t) = \frac{\Gamma}{4\pi}\int_{-\pi}^{\pi}\left(\frac{\partial\mathbf{X}}{\partial\xi} \wedge \frac{\mathbf{X}(\xi_0,t)-\mathbf{X}(\xi,t)}{\{|\mathbf{X}(\xi_0,t)-\mathbf{X}(\xi,t)|^2+\mu^2\}^{\frac{3}{2}}} - \left(\frac{\partial\mathbf{X}}{\partial\xi}\right)_0 \wedge \left(\frac{\partial^2\mathbf{X}}{\partial\xi^2}\right)_0 P(\xi,t)\right) d\xi$$
$$+\frac{\Gamma}{4\pi}\left(\frac{\partial\mathbf{X}}{\partial\xi}\right)_0 \wedge \left(\frac{\partial^2\mathbf{X}}{\partial\xi^2}\right)_0 \int_{-\pi}^{\pi} P(\xi,t)\,d\xi. \tag{3.8}$$

The integrand in the first integral is $O(1)$ everywhere while the second integral is elementary.

In view of the uniformity of the cross-section and conservation of volume,

$$\mu(t) = 2\delta_R c_0\left\{\frac{1}{L_0}\int_{-\pi}^{\pi}\left|\frac{\partial\mathbf{X}}{\partial\xi}\right| d\xi\right\}^{-\frac{1}{2}} \tag{3.9}$$

where L_0 and c_0 are the respective initial values of the length and core radius of the vortex ring. For an ellipse

$$L_0 = 4aE(e) \tag{3.10}$$

where e is the eccentricity of the ellipse, $e^2 = (a^2-b^2)/a^2$, and $E(e)$ is the complete elliptic integral of the second kind (see appendix A for definition).

Once the values of A and c_0 are given, equations (3.8), (3.6), (3.9) and (3.5) completely specify the initial value problem and the evolution of the vortex ring can be determined numerically. The interval $(-\pi, \pi)$ was divided into $4(N-1)$ portions by $4N-3$ equally spaced grid points. The spatial derivatives were calculated using four-point centred differences and Simpson's rule was used to carry out spatial integration.

Because of its stability, the fourth-order Runge–Kutta formula was used to carry out the integration forward in time.

The calculations were carried out for four different eccentricities of the initial elliptic ring and the results are described in the next section.

4. Numerical results

The equation of motion is made dimensionless by choosing the semi-major axis a as the unit of length and $4\pi a^2/\Gamma$ as the unit of time. Thus the dimensionless time t_1 is given by

$$t_1 = \frac{\Gamma}{4\pi a^2} t. \tag{4.1}$$

Before calculations can be performed, the value of A in (3.2) and the initial value of the core radius c_0 are needed. These depend on the process of generation of the vortex ring. One method of generation in an ideal fluid is to give an impulse to a flat disk of elliptic shape and then to dissolve it away. By equating the energy and impulse of the disk to that of the resulting vortex ring, in the manner of Taylor (1953), the core size and the circulation of the vortex ring can be evaluated. The details are pursued in appendix A. The initial distribution of potential at the edge of the disk given by (A 2) suggests that in the core of the resulting vortex ring the appropriate distribution of velocity to take is

$$v = \frac{\Gamma}{2\pi(cr)^{\frac{1}{2}}}, \quad w = 0, \tag{4.2}$$

where v and w are respectively the azimuthal and axial velocities relative to the centre of the core and r is the radial distance from it. This implies that in (3.3) $f = (r/c)^{\frac{1}{2}}$ so that

$$A = 1. \tag{4.3}$$

The initial core radius is given by (A 11). For the cases considered here the values are tabulated below (table 1); the case $b/a = 1$ is also included.

The radius of curvature ρ of an ellipse varies from a value b^2/a at the major axis to a value a^2/b at the minor axis. The maximum and minimum values of c_0/ρ are also shown in table 1.

These values are not small as required by the cut-off theory. However, in the absence of axial flow, the error in the cut-off approximation is of the same order in c_0/ρ as in Saffman's (1970) formula for the velocity of a circular vortex ring. By comparing with numerical calculations of the full equations of motion, Fraenkel (1970) and Norbury (1973) have shown that Saffman's formula is fairly good for values of c_0/ρ which are not small compared with unity. Thus, although no rigorous proof is available, it is reasonable to expect that the cut-off theory will hold equally good for such values of c_0/ρ.

In any case the results are not sensitive to the precise value of c_0/ρ since the velocity obtained from the cut-off theory depends only logarithmically on the cut-off length and hence the radius of the core. Thus, as far as the motion of the centre-line of the vortex ring is concerned, the results obtained here are applicable, within a small error, to a vortex ring of the same configuration but smaller core size. Only those inferences which depend directly on the core size will differ.

b/a	c_0/a	$(c_0/\rho)_{\max} = c_0 a/b^2$	$(c_0/\rho)_{\min} = c_0 b/a^2$
0·2	0·109	2·73	0·022
0·4	0·207	1·29	0·083
0·6	0·287	0·797	0·172
0·8	0·347	0·542	0·278
1·0	0·393	0·393	0·393

TABLE 1. Predicted core-size of vortex ring produced by the process described in appendix A.

b/a	N	Δt_1
0·2	41	0·0001
0·4	41	0·001
0·6	41	0·001
0·8	21	0·002

TABLE 2. Number of points per quadrant and time step used.

Table 2 shows the values of N and time step Δt_1 used in each of the cases considered. Trial and error showed that these gave adequate accuracy. Smaller time steps were needed with increasing eccentricity of the initial ellipse because of the rapid changes associated with the large curvature at the major axis.

In view of the results of § 2, it is anticipated that in the case of small eccentricity the vortex ring will oscillate with a period given by (2.3). As a check on the computer program, this was verified. In order to measure the oscillations, an amplitude B is defined and monitored together with the variance of the points on the ring from a plane parallel to the plane of the original ellipse and moving with the velocity of the centroid of the ring. If $\mathbf{I}$ is the impulse of the vortex ring, the centroid is given by (Saffman 1970)

$$\overline{\mathbf{X}}(t_1) = \frac{\Gamma}{2}\oint \frac{(\mathbf{X}\wedge\hat{\mathbf{t}}.\mathbf{I})}{\mathbf{I}^2}\mathbf{X}\,ds \tag{4.4}$$

where $\hat{\mathbf{t}}$ is the unit tangent to the filament, so that for a ring which is symmetric about $x = 0$ and $y = 0$ in Cartesian co-ordinates fixed in the plane of the original ellipse,

$$\overline{\mathbf{X}}(t_1) = \left(0, 0, \frac{1}{2\pi ab}\oint\left(x\frac{dy}{ds} - y\frac{dx}{ds}\right)z\,ds\right) \tag{4.5}$$

since $I = \Gamma\pi ab$ is conserved. (This was checked by evaluating I at various times during the calculations.) Then amplitude B is defined as

$$B = \frac{A_1 - B_1}{A_1 + B_1} \tag{4.6}$$

where

$$A_1(t_1) = \max|\,\mathbf{X}(\xi, t_1) - \overline{\mathbf{X}}(t_1)\,|,$$

$$B_1(t_1) = \min|\,\mathbf{X}(\xi, t_1) - \overline{\mathbf{X}}(t_1)\,|.$$

The variance Σ is defined as

$$\Sigma(t_1) = \frac{1}{2\pi a^3 b}\oint\left(x\frac{dy}{ds} - y\frac{dx}{ds}\right)(z-\bar{z})^2\,ds \tag{4.7}$$

where $\bar{z}(t_1) = \overline{\mathbf{X}}.\mathbf{k}$.

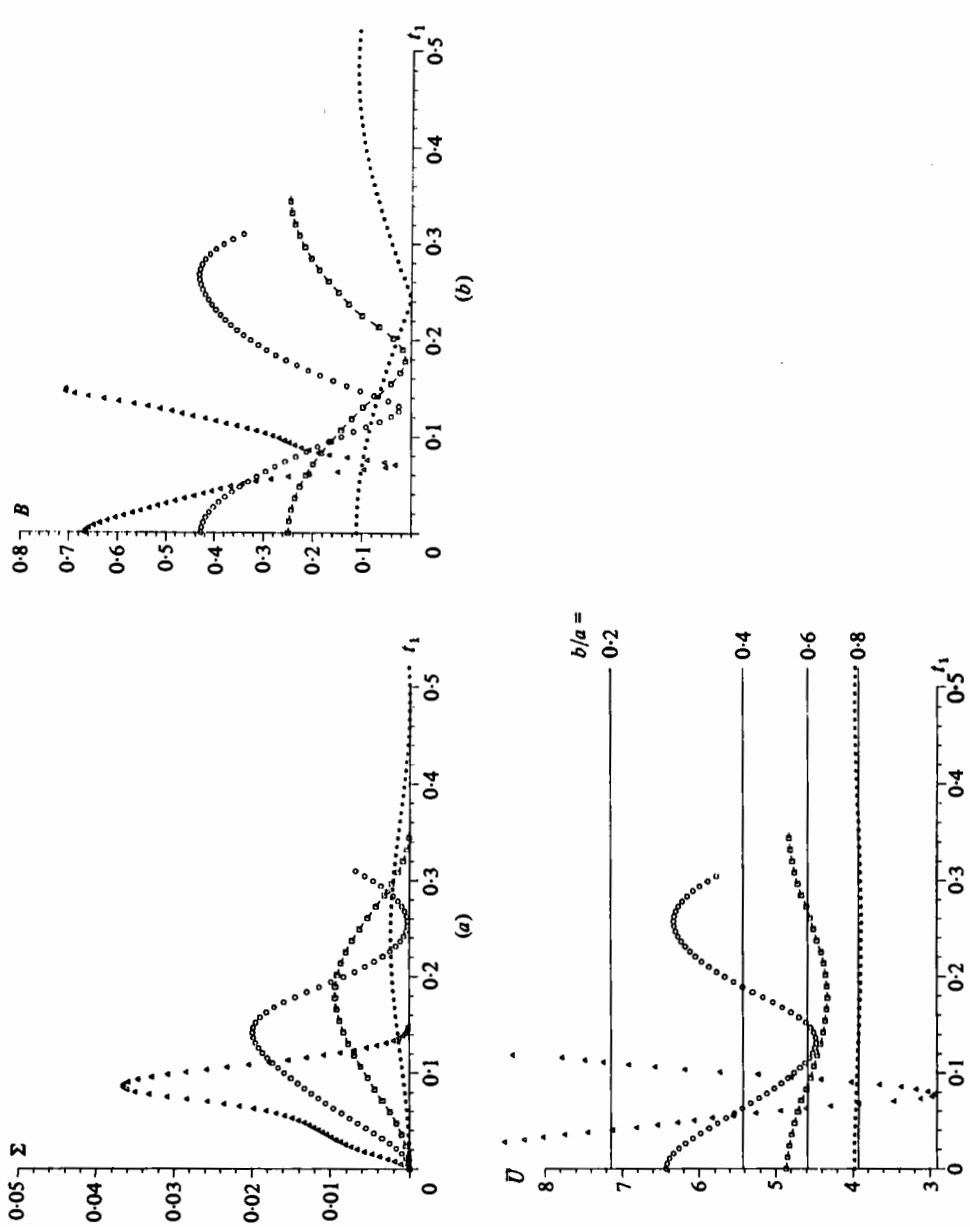

FIGURE 1. Plot of (*a*) variance $\Sigma(t_1)$ *vs.* t_1, (*b*) amplitude $B(t_1)$ *vs.* t_1 and (*c*) centroid velocity $\bar{U}(t)$ *vs.* t_1 for cases $b/a = 0{\cdot}2(\Delta)$, $0{\cdot}4(\bigcirc)$, $0{\cdot}6$ $(\square)$ and $0{\cdot}8$ $(*)$. The solid lines in (*c*) give velocity $V_L(\frac{1}{2}(a+b), c_0, 1)$.

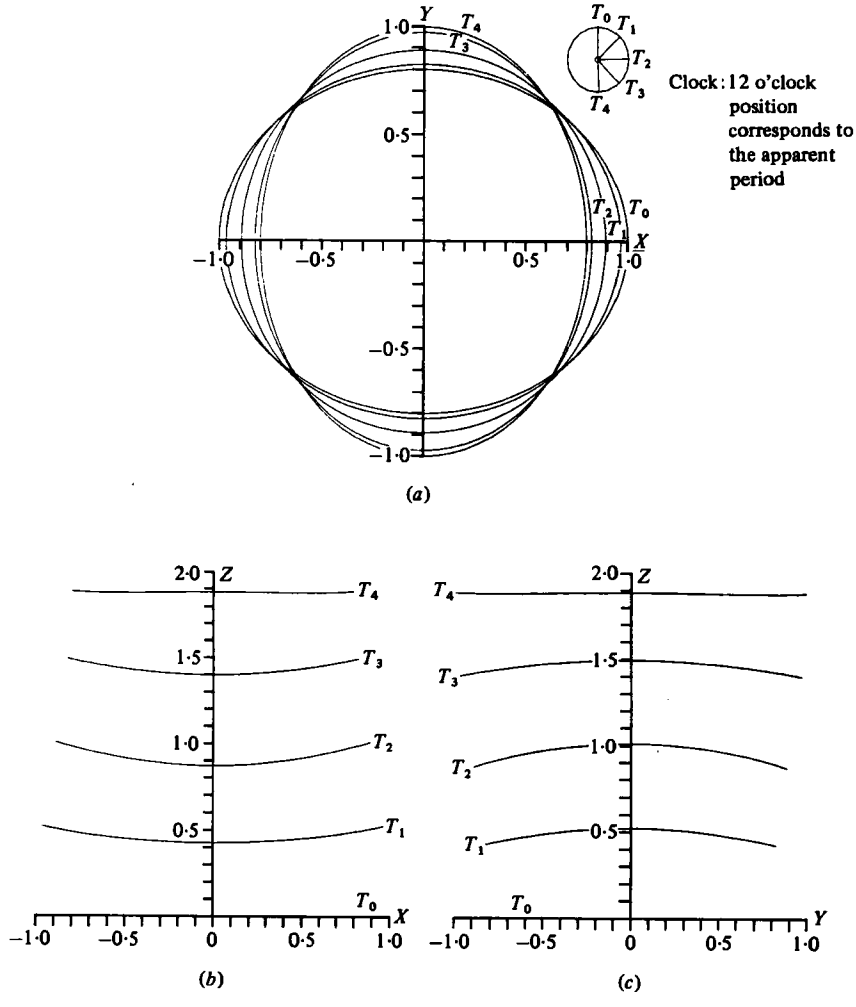

FIGURE 2. Evolution of the elliptic vortex ring of axes ratio 0·8.
(*a*) Plan view, (*b*) side view, (*c*) end view.

The values of $\Sigma(t_1)$ and $B(t_1)$ have been plotted against time in figure 1 (a, b). Initially, when the vortex ring is flat and elliptic in shape, Σ is zero and $B = (a-b)/(a+b)$. Subsequently, Σ and B oscillate in time. For $t_1 > 0$, Σ first achieves a minimum at a time defined as $t_1 = \frac{1}{2}\tau_A$. Except in the case of $b/a = 0{\cdot}8$ the value of the minimum is different from zero; the difference is small but not negligible. Thus at $t_1 = \frac{1}{2}\tau_A$, the vortex ring is flat in the case $b/a = 0{\cdot}8$ and nearly so in the other cases considered. The numerical calculations were stopped just after $t_1 = \frac{1}{2}\tau_A$.

For the $b/a = 0{\cdot}8$ case the shape of the centre-line of the vortex ring at various instants of the evolution is shown in figure 2. At $t_1 = \frac{1}{2}\tau_A$, as expected from the value of $\Sigma(\frac{1}{2}\tau_A)$, the vortex ring is flat. It is also elliptic in shape with the orientation of its axes reversed. Thus in this case the vortex ring oscillates periodically since it can be rotated through an angle of 90° to obtain the initial configuration. The time $\frac{1}{2}\tau_A$ is in good agreement with the half-period of oscillation of an equivalent perturbed circular

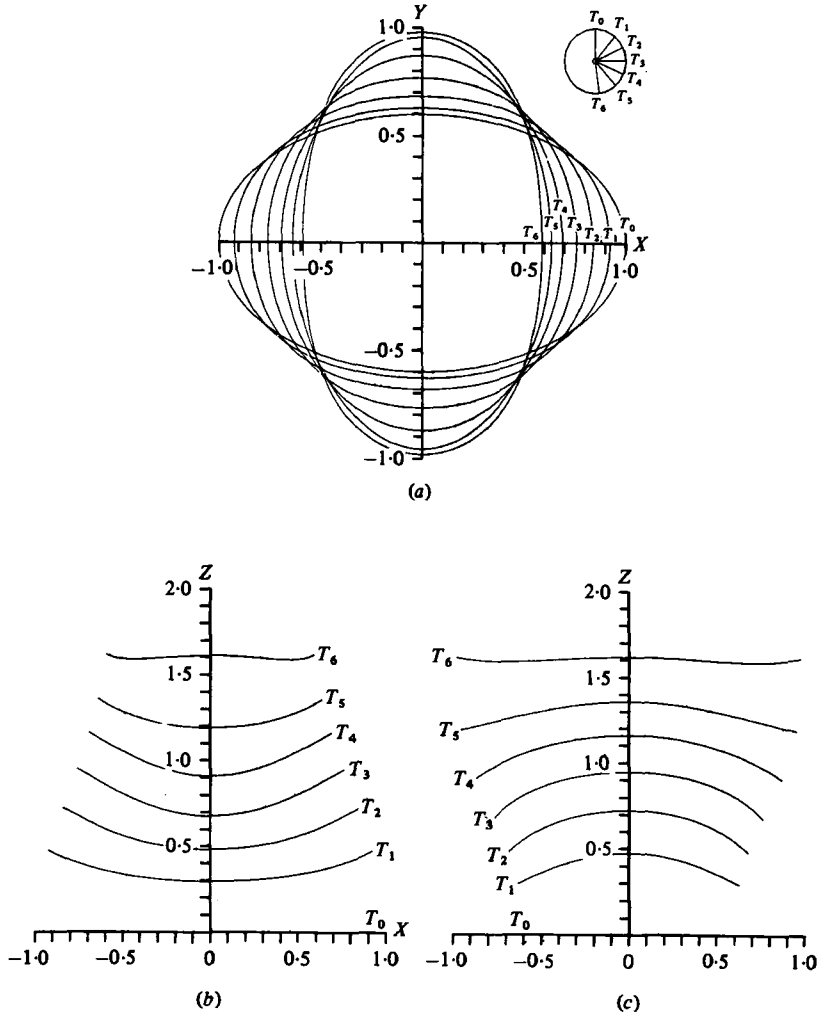

FIGURE 3. Evolution of the elliptic vortex ring of axes ratio 0.6.
(*a*) Plan view, (*b*) side view, (*c*) end view.

vortex ring of radius $R = 0{\cdot}9a$, given by $\frac{1}{2}((\Gamma/4\pi a^2)\tau(0{\cdot}9a, 0{\cdot}347, 1))$, where τ is as in (2.3).

In the other more eccentric cases considered, the vortex ring assumes complicated forms during the evolution.

For the $b/a = 0{\cdot}6$ and $0{\cdot}4$ cases, the different stages of the evolution are shown in figure 3 and figure 4 respectively. At $t_1 = \frac{1}{2}\tau_A$, as expected from $\Sigma(\frac{1}{2}\tau_A)$, the vortex ring is not exactly flat. Nor is the shape of the vortex ring elliptic, although the orientation of the axes is reversed as in $b/a = 0{\cdot}8$ case. After $t_1 = \frac{1}{2}\tau_A$, the vortex ring starts deforming in such a way that the axes tend to attain their initial orientation. Thus, although the vortex ring oscillates, the oscillations are not periodic in these cases. Thus a flat elliptic vortex ring is not, in general, a periodic solution of the vortex ring configurations. τ_A will be referred to as the 'apparent period' of oscillation of the elliptic vortex ring.

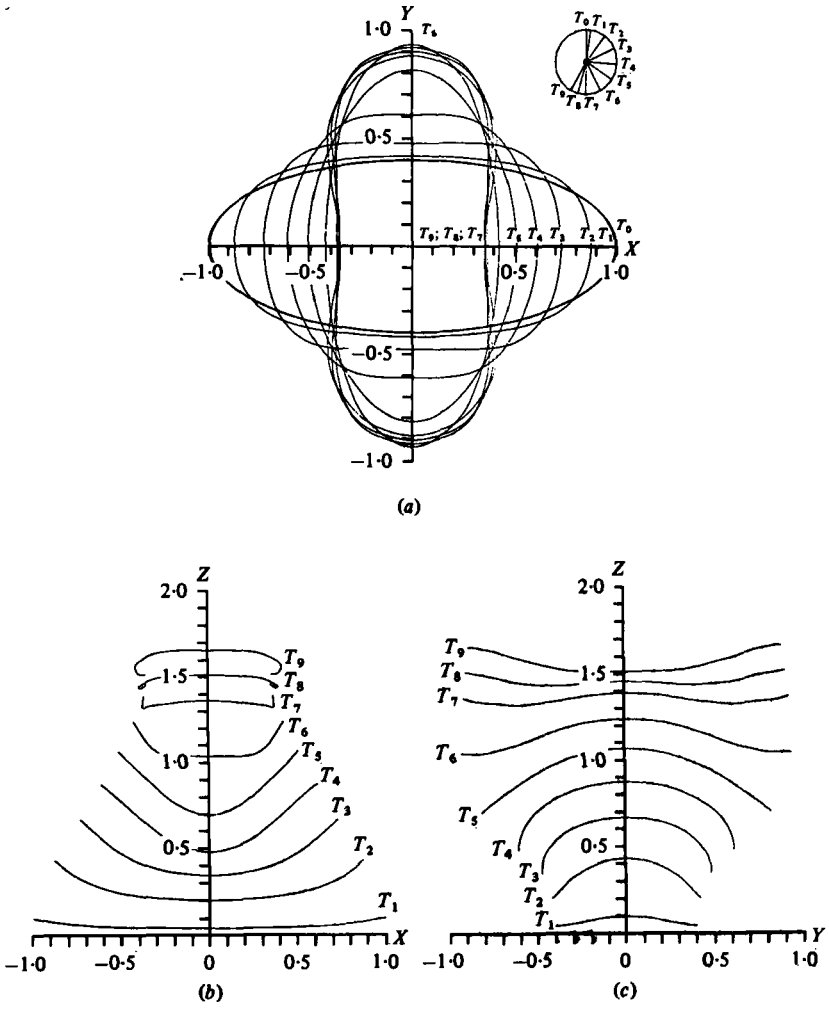

FIGURE 4. Evolution of the elliptic vortex ring of axes ratio 0·4.
(*a*) Plan view, (*b*) side view, (*c*) end view.

The different stages of evolution of the vortex ring in the case $b/a = 0{\cdot}2$ are shown in figure 5. In this case at $t_1 = 0{\cdot}1355$ ($< \frac{1}{2}\tau_A$), the points on $y = 0$ are $0{\cdot}214a$ distance apart, which implies that the cores are touching. Since the calculations are based on the assumption that the separation of such points on the vortex ring is large compared with the core radius, the results at this stage may be viewed with scepticism. However, by performing a numerical calculation with vortices in two-dimensions, in which the core was allowed for, Moore (1972) was able to show that the Biot–Savart formula gives roughly the correct velocity even when the cores are touching. Thus, as Moore points out, it is expected that, while the cores will be distorted so that the cut-off length will change, the approximations on which the present calculations are based will be reasonably adequate even when the cores are close to each other.

The relevance of the calculations to the real situation at the instant of touching is difficult to assess. However, experiments, due to Fohl & Turner (1975), Oshima &

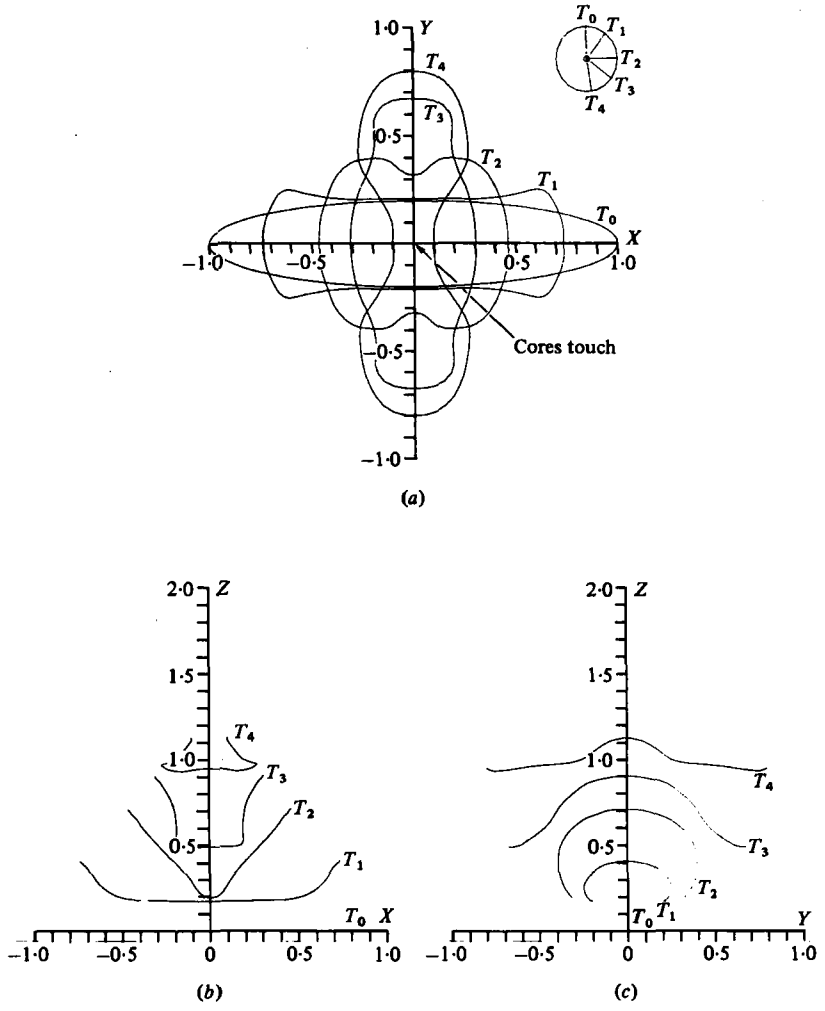

FIGURE 5. Evolution of the elliptic vortex ring of axes ratio 0·2.
(*a*) Plan view, (*b*) side view, (*c*) end view.

Asaka (1977*a*, *b*) and Oshima (1978), with colliding vortex rings suggest that since the vortex cores, where they touch, have vorticity of opposite sign, viscous diffusion would annihilate the vorticity locally. Although the actual process is complicated, the net result would be that the vortex lines would connect on either side of the region of contact to form two smaller rings.

It is not meaningful to continue with the numerical integration beyond the approximate instant of touching. However, in order to obtain an estimate of the nearest distance of approach of the core centres, it was decided to carry the integration forward in time as far as possible using the same number of points and time step. Numerical instability sets in near $y = 0$ at $t_1 = 0{\cdot}15$ when the two centre-line points on $y = 0$ are $0{\cdot}014a$ distance apart. The instability is presumably due to this separation distance being small compared with the grid spacings and could be remedied by using smaller grid spacings and smaller time step. However, this was not attempted in view of the

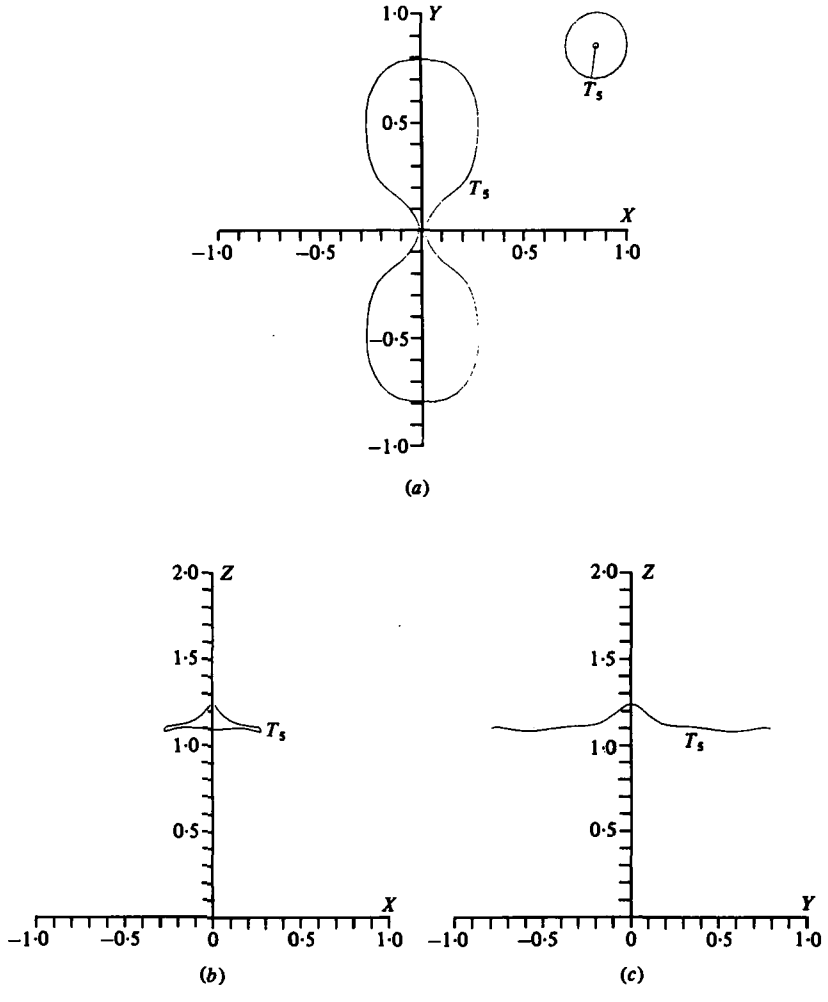

FIGURE 6. Shape of the vortex ring of case $b/a = 0{\cdot}2$ at $t_1 = 0{\cdot}149$ ($> \frac{1}{2}\tau_A$). (*a*) Plan view, (*b*) side view, (*c*) end view.

dubious implication of the results at this stage. The shape of the centre-line of the ring at $t_1 = 0{\cdot}149$ is shown in figure 6.

At $t_1 = \frac{1}{2}\tau_A (= 0{\cdot}147)$, the separation of the two centre-line points on $y = 0$ is $0{\cdot}05a$. The overall length is greater by 2% over its initial value so that the core size is not significantly different from its initial value. Thus, within logarithmically small error, it appears that an elliptic vortex ring of axes ratio 0·2 and core radius c_1 such that $c_1 > 0{\cdot}025a$ would break up into smaller rings before the apparent half-period stage is reached.

The values of $\tau_N = a\tau_A/b$ for the cases considered are shown in table 3. The reason for tabulating τ_N instead of τ_A is that it is less dependent on the impulse of the vortex ring than τ_A. τ_N is in good agreement with

$$\tau_L = \frac{\Gamma}{4\pi ab}\tau\left(\frac{a+b}{2}, c_0, 1\right) \tag{4.8}$$

b/a	$\tau_N = \frac{a\tau_A}{b}$	τ_L	$\bar{\bar{U}}$	V_L
0·8	1·213	1·212	3·935	3·925
0·6	1·220	1·217	4·522	4·506
0·4	1·290	1·244	5·564	5·425
0·2	1·47	1·432	7·383	7·142

TABLE 3. Apparent period of oscillation τ_N and mean velocity $\bar{\bar{U}}$ compared with τ_L and V_L respectively.

where τ is given by (2.3) and c_0 is tabulated in table 1. For comparison, the values of τ_L are also shown in table 3.

It may be of interest to note that the velocity $\bar{U}$ of the centroid of the ring, defined by

$$\bar{U} = \frac{d\bar{z}}{a\,dt_1} \tag{4.9}$$

where $\bar{z}$ is given by (4.7), oscillates in time about a mean value $\bar{\bar{U}}$ with an apparent period approximately equal to $\frac{1}{2}\tau_A$. A plot of $\bar{U}$ against time is shown in figure 1(*c*). $\bar{\bar{U}}$ is in good agreement with the velocity of an equivalent circular vortex ring,

$$V_L = \frac{4\pi a}{\Gamma} V\left(\frac{a+b}{2}, c_0, 1\right) \tag{4.10}$$

where V is given by (2.5). For comparison, the values of $\bar{\bar{U}}$ and V_L for the cases considered are shown in table 3.

5. Experimental measurements

The elliptic vortex rings were produced by puffing air through sharp-edged elliptic orifices of the same eccentricities as those used in the numerical calculations. Each orifice, of semi-major axis a_0, was cut in a thin plate of 14 cm diameter which was mounted on one end of a 70 cm long perspex tube of the same diameter. The other end of the tube was smoothly connected to a 8·3 cm diameter brass cylinder which contained the piston (figure 7). The piston was driven, through a gearbox, by a high torque stepping motor which was operated by a logic control circuit. With this arrangement it was possible to provide high initial and terminal accelerations with a uniform velocity over most of the piston stroke. The acceleration and deceleration times, the top piston speed and the length of the stroke could be easily adjusted. In order to provide draught-free conditions, the vortex rings were produced in a 40 × 40 × 70 cm perspex box. The arrangement made it possible to obtain reproducible vortex rings.

The experiment consisted of hot-wire anemometer measurements to determine the circulation and core size and flow visualization studies to determine the mean translational velocity $\bar{U}_E$, the equivalent ring radius R_0 and the oscillatory features of the vortex rings.

Glycerine smoke was used to provide flow visualization. The motion of the vortex rings was recorded on a 16 mm ciné film at 32 frames/s and 64 frames/s. The film was analysed to determine the characteristics of the motion of the ring. Starting from the moment of generation, the maximum y-displacement (see figure 7), y_M, of the vortex

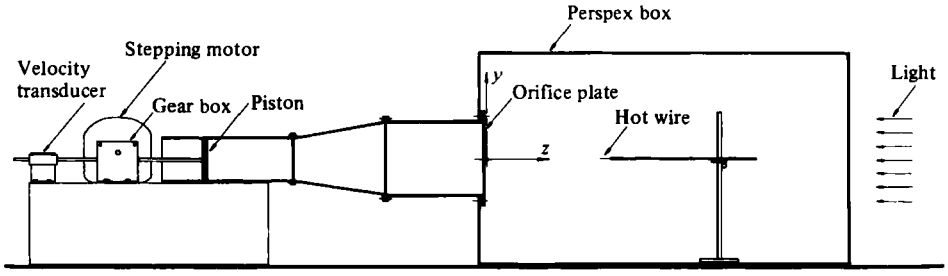

FIGURE 7. Experimental set-up.

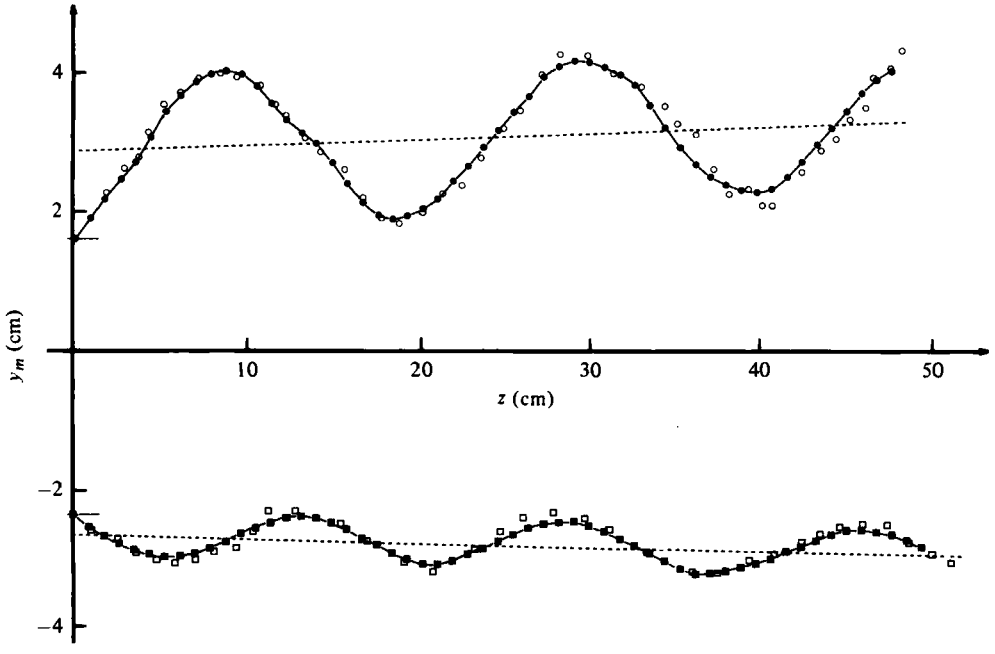

FIGURE 8. Plot of y_M *vs.* distance from the orifice. In the upper half positive y_M is plotted for $b/a = 0{\cdot}6$ case and in the lower half negative y_M is plotted for $b/a = 0{\cdot}8$ case. The unshaded symbols ○ and □ refer to values obtained from a single run while the corresponding shaded symbols refer to averaged values.

ring was recorded and Fourier-analysed. Plots of y_M for the cases 0·6 and 0·8 are shown in figure 8; the figure also shows the average values of the y_M over five different runs. The ends of an oscillation cycle were defined to be the times when y_M was a minimum and the time interval between the ends of a oscillation was defined as the oscillation time $\tilde{\tau}_E$, to be compared with the corresponding apparent period τ_A of §4.

A survey of the velocity field in a plane parallel to the plane of the orifice and at a fixed distance from it was made by recording hot-wire anemometer signals at various positions in the plane. At each position, several different recordings were made; for each recording, a vortex ring was produced, checking that the piston velocity had the same value each time. For a circular vortex ring, a few hot-wire traces are needed (Sallet & Widmayer 1974) to obtain a qualitative description of the flow field.

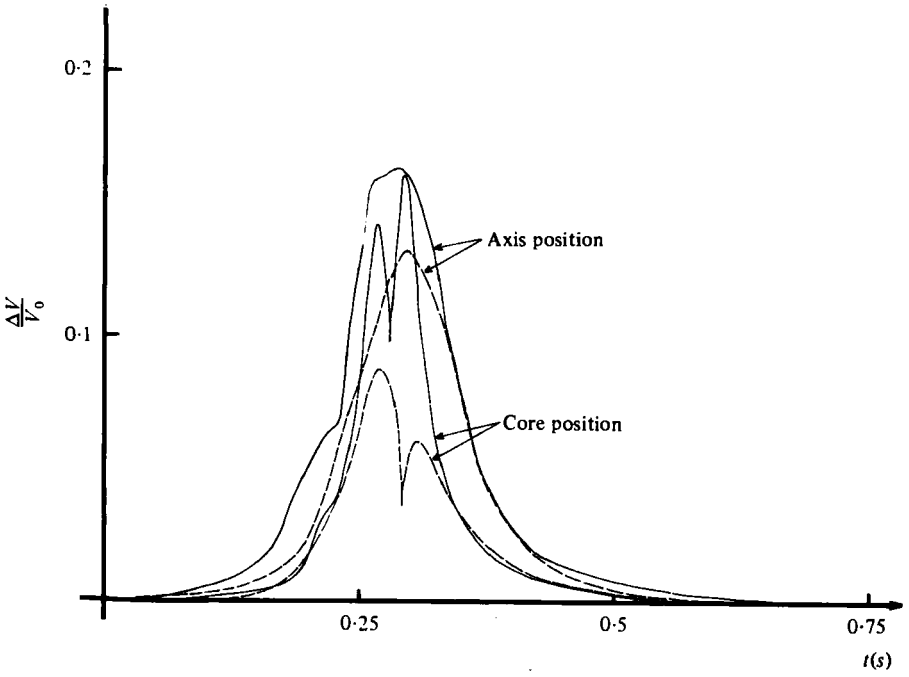

FIGURE 9. Non-dimensional voltage output from the hot-wire anemometer, placed 10 cm. from the orifice, plotted against time. ----, $b/a = 0{\cdot}8$; ——, $b/a = 0{\cdot}4$.

However, in the present case the vortex ring is deforming as it moves and traces at several positions are needed. The order of the difficulty of the analysis increases when more eccentric cases are considered. The measurements were repeated at a further distance from the orifice.

From the available traces, the ones corresponding to the axis of the ring and the centre of the core were identified (see Sallet & Widmayer). For the $b/a = 0{\cdot}8$ and $b/a = 0{\cdot}4$ cases, these are shown in figure 9. The core-position trace was used to determine the core size of the ring. From the axis-position trace, the velocity component u along the z-axis can be determined (by symmetry the other components are zero). This enables (see, for example, Didden 1977) the circulation Γ to be determined: within a closed curve C containing the vortex core, Γ is found by integrating the velocity along the z axis and closing the curve C outside the z axis at infinity where u and v (y-velocity component, say) are zero. Thus

$$\Gamma = \oint_C (u\,dz + v\,dy) = \int_0^\infty u(z, y = 0)\,dz = \int_0^\infty u\,\bar{U}_E\,dt, \tag{5.1}$$

where the transformation $dz = \bar{U}_E\,dt$ has been used. From the ciné film, $\bar{U}_E$ is determined by analysing the end view of the evolution as the average of the z-velocity of the projection on the y–z plane of these points on the vortex ring which lie in its planes (fixed) of symmetry. The velocity at each of these points on the vortex ring is obtained by noting its instantaneous z-displacement and numerically differentiating it with respect to time. The oscillatory behaviour of $\bar{U}_E$, anticipated by the numerical

Axes ratio $b_0/a_0 = b/a$	Semi-major axes of orifice, a_0 (cm)	L (cm)	W (cm s^{-1})	a (cm)	$R = a + \frac{1}{2}b$ (cm)	C_E/a	Γ (cm^2 s^{-1})
0·8	3·1	0·7	11·7	3·38	2·95	0·33	390
0·6	4	1·4	11·5	4·44	3·55	0·31	332
0·4	4	1·2	9·1	4·61	3·22	0·32	370
0·2	4	0·4	4·0	4·72	2·83	0·23	196

TABLE 4. Estimates of vortex parameters predicted by method given in appendix B.

$b_0/a_0 = b/a$	a (cm)	$R = a + \frac{1}{2}b$ (cm)	C_E/a	$\tilde{V}$ (cm s^{-1})	Γ (cm^2 s^{-1})	$Re = \Gamma/\nu$
0·8	3·17	2·85	0·31 ± 0·07	3·0	407	2714
0·6	4·37	3·5	0·25 ± 0·05	2·8	437	2914
0·4	4·28	2·95	0·29 ± 0·05	2·7	471	3140
0·2	—	—	0·26 ± 0·05	3·0	211	1473

TABLE 5. Measured values of vortex parameters.

calculations, was noticeable only in the more eccentric cases and appeared in the form of fluctuations approximately about $\overline{\overline{U}}$ (defined in §4).†

To obtain estimates of the vortex parameter it is not satisfactory to model the flow by a uniform flow past an equivalent disk and use the method described in appendix A; see e.g. Sallet (1975). Instead, the estimates are obtained using a model of the flow, given by Saffman (1978), in which it is assumed that when the flow is first set into motion, the vortex sheet at the orifice behaves locally like a two-dimensional vortex sheet formed at the edge of a semi-infinite plate. Then applying the similarity law for the roll up of the vortex sheet and using the estimates given by Pullin (1978) for the constants associated with the law, it is possible to obtain estimates of the circulation Γ, the length of the axes and the core size of the ensuing elliptic vortex ring. The details are given in appendix B and the estimates for the circulation Γ, the semi-major axis a, the equivalent radius R and core size C_E for the cases considered are given in table 4. Here L and W refer to the displacement and velocity respectively of an equivalent slug of fluid in the perspex cylinder (see figure 7). The flux of fluid through a cross-section of the slug is equated to the flux through the orifice. The fluid velocity in the perspex cylinder was checked and found to be approximately uniform over the time of the stroke. For comparison, the corresponding measured values are given in table 5 where $Re\,(= \Gamma/\nu)$ is the vortex Reynolds number and $\tilde{V} = 4\pi\overline{\overline{U}}R/\Gamma$.

6. Comparison of numerical and experimental results

Figure 10 shows the contrast between a vortex ring produced from a circular orifice and that produced from an elliptic orifice of axes ratio 0·4.

For axes ratios $b/a = 0{\cdot}8$, 0·6 and 0·4, the vortex ring was observed to oscillate in the manner anticipated by the numerical calculations. In fact, qualitative comparisons between some of the stills of the vortex ring from the ciné film and the computed

† The oscillations in the mean velocity as well as in an amplitude corresponding to y_m were also observed by Oshima (1972) in the case of vortex rings produced in water from a lenticular orifice.

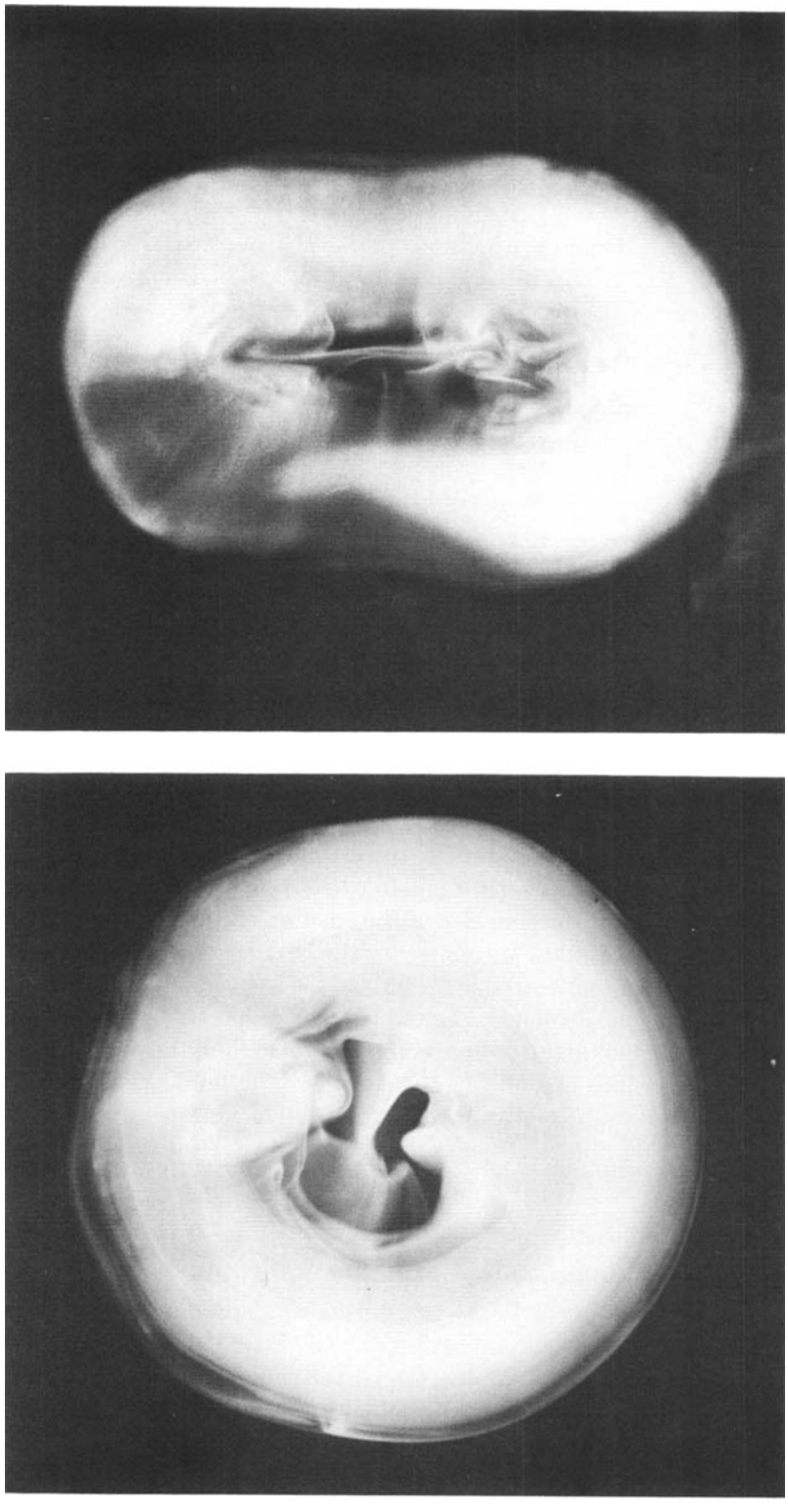

FIGURE 10. Comparison between an evolving vortex ring and a non-evolving vortex ring.

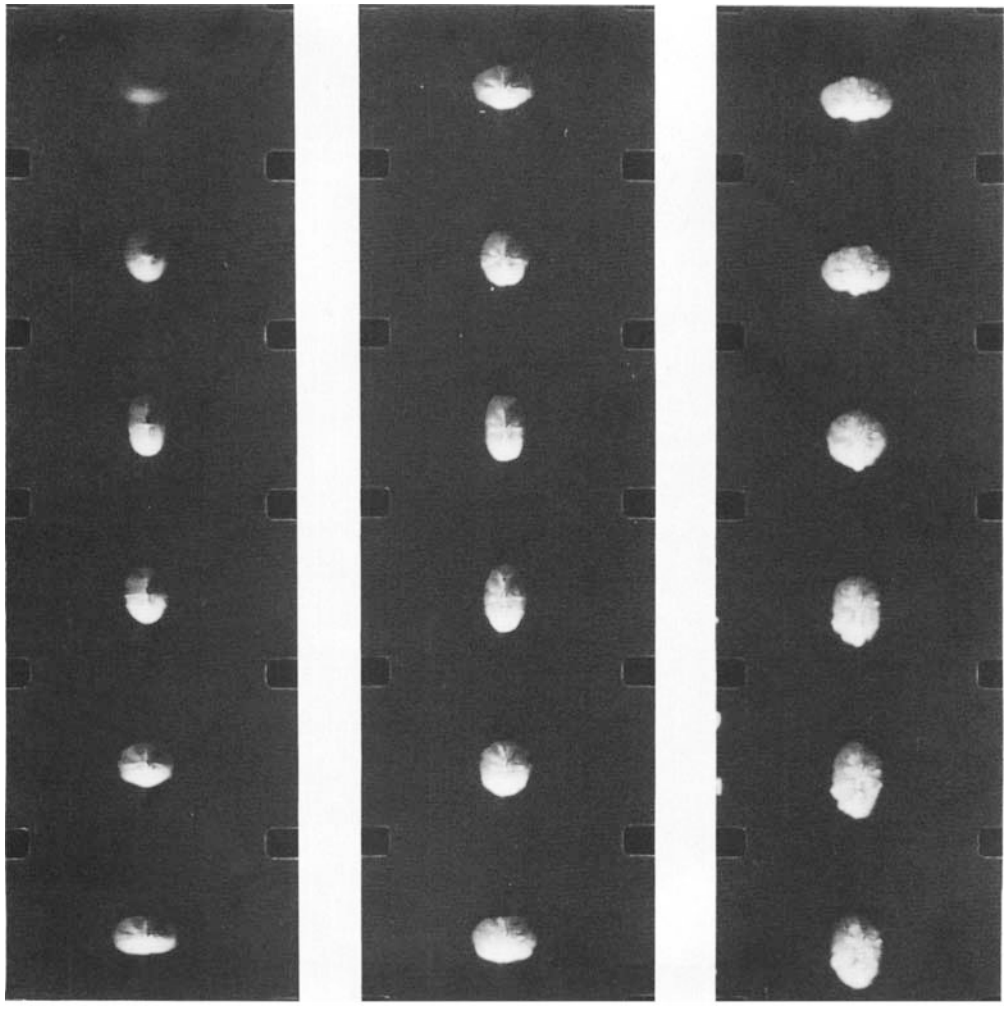

FIGURE 11. The plan view of the evolution of an elliptic vortex ring of axes ratio 0·4. The order of the sequence is from top to bottom and left to right. The top left-hand frame shows the vortex ring just forming. The major axis of the orifice is in the horizontal direction. The film sequence was taken at 32 frames/s.

configurations in figures 2–4 showed striking resemblence. Figure 11 shows the plan view of the evolution of the vortex ring for the case $b/a = 0{\cdot}4$. As may be noticed from the figure, at the end of the first half cycle the vortex ring assumes the shape shown in figure 4 for time T_7. This shape was observed at each subsequent end of cycle for three cycles indicating that this configuration may be a possible periodic solution of the vortex ring. The contortions seen in the photograph in the set of frames on the far right in figure 11 are a defect of the photography and do not indicate a short-wave instability of the ring; the vortex ring has progressed beyond the depth of focus of the camera. However, a short-wave instability of the type described by Widnall & Tsai (1977) for a circular vortex ring was eventually observed for the $b/a = 0{\cdot}4$ case; figure 12 shows eight waves growing on the elliptic vortex ring. The pictures were taken at approximately 1s after generation time. From Saffman's (1978) formula

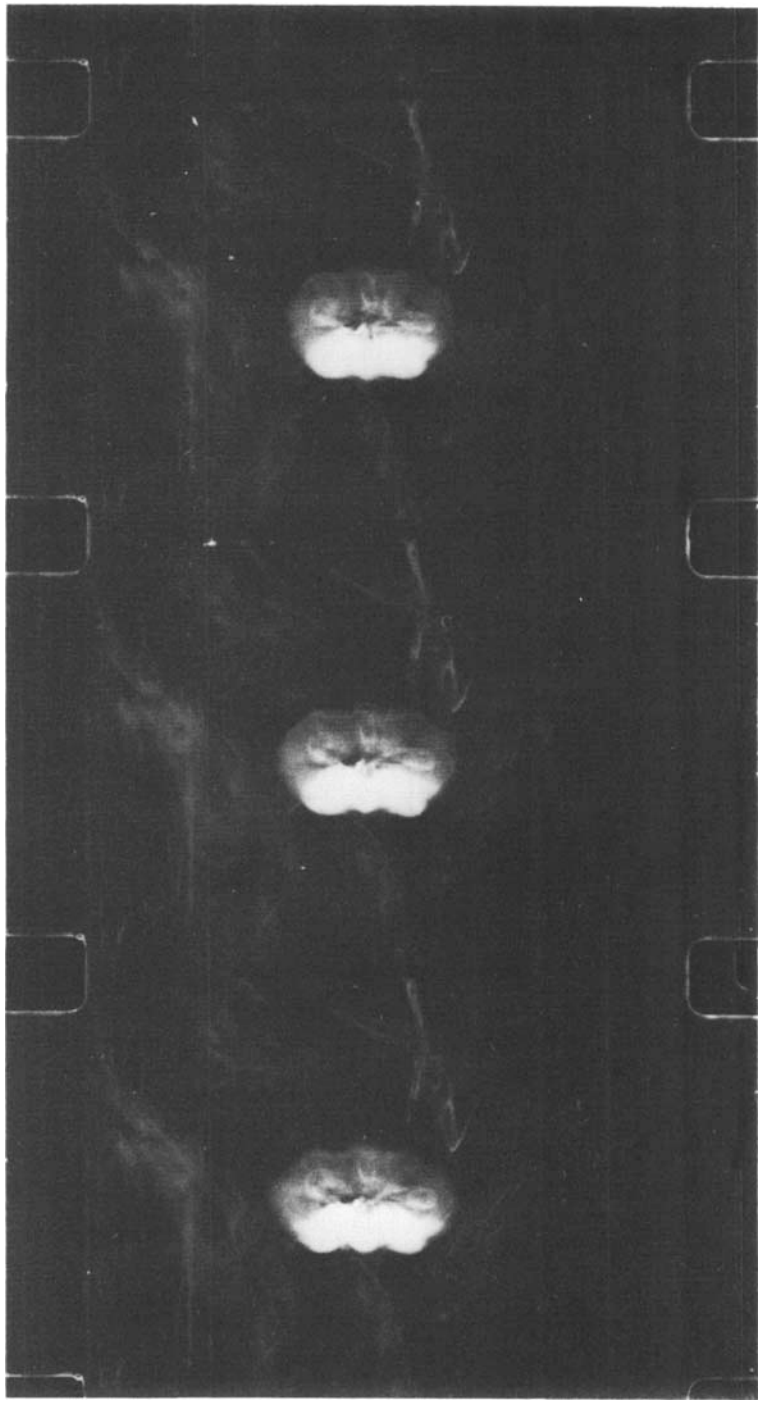

FIGURE 12. Vortex ring in the case $b/a = 0{\cdot}4$ at the end of third oscillation showing short-wave instability. The sequence was taken at 32 frames/s.

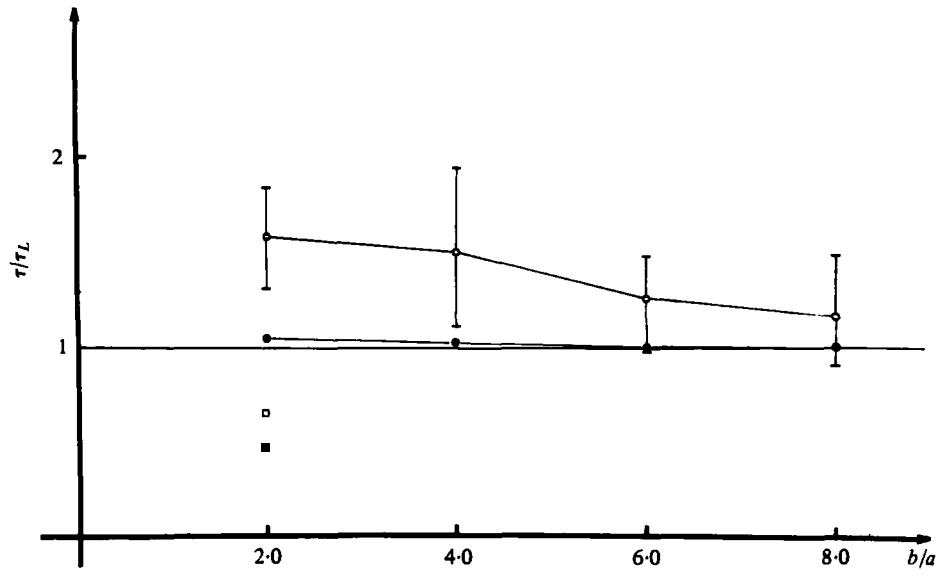

FIGURE 13. Plot of τ/τ_L against axes ratio b/a. The symbol ○ refers to τ_E/τ_L ($\frac{1}{2}(a+b)$, C_E, 1); the standard errors for these experimental values are also shown. The ● refers to τ_N/τ_L ($\frac{1}{2}(a+b)$, c_0, 1). For $b/a = 0{\cdot}2$, the corresponding times of the break-up of the ring are shown by □ and ■ respectively.

(2·18) with $\epsilon = 0{\cdot}62$ and $R = 2{\cdot}95$ cm (see table 5) and using his equations (3·6), the expected number of waves N on an equivalent circular vortex ring is $N = 8$ approximately. The agreement is remarkably good considering that the observed vortex ring is not circular.

It was found that in each case considered, the oscillation time $\tilde{\tau}_E$ had a greater value for each subsequent cycle. This increase in $\tilde{\tau}_E$ with time is believed to be related to the accompanying increase in the equivalent radius of the ring observed at the end of each oscillation cycle. For the purpose of comparison with numerical computations

$$\tau_E = \frac{a\tilde{\tau}_E}{b}, \tag{6.1}$$

is defined. The values of $\frac{1}{2}\tau_E$ for the first half cycle is compared with the corresponding numerical values of $\frac{1}{2}\tau_N$ in figure 13. It is found desirable to plot τ_E/τ_L ($\frac{1}{2}(a+b)$, C_E, 1) and τ_N/τ_L ($\frac{1}{2}(a+b)$, c_0, 1), instead of τ_E and τ_N in view of the differences in core size between that used in the computations and the corresponding observed value. The results are in fair agreement in the cases $b/a = 0{\cdot}8$ and $0{\cdot}6$. For the case $b/a = 0{\cdot}4$, the value of τ_E/τ_L is much greater than τ_N/τ_L. However, the error margin in the value of τ_E/τ_L is large. This is due to the difficulty in ascertaining the value of Γ as a result of the high fluctuations in $\overline{U}_E$ observed in this case.

In the case $b/a = 0{\cdot}2$, the vortex ring was observed to break up into two smaller rings as anticipated in §4, provided the Reynold's number of the flow was high enough ($\Gamma/\nu > 1300$ approximately). Figure 14 shows the end view of the break-up process. The shape of the vortex ring prior to the break-up may be compared with the configurations shown in figure 5(*c*). After break-up, the two ensuing vortex rings are observed to oscillate and travel in directions inclined at equal angles to the z axis; the size of the

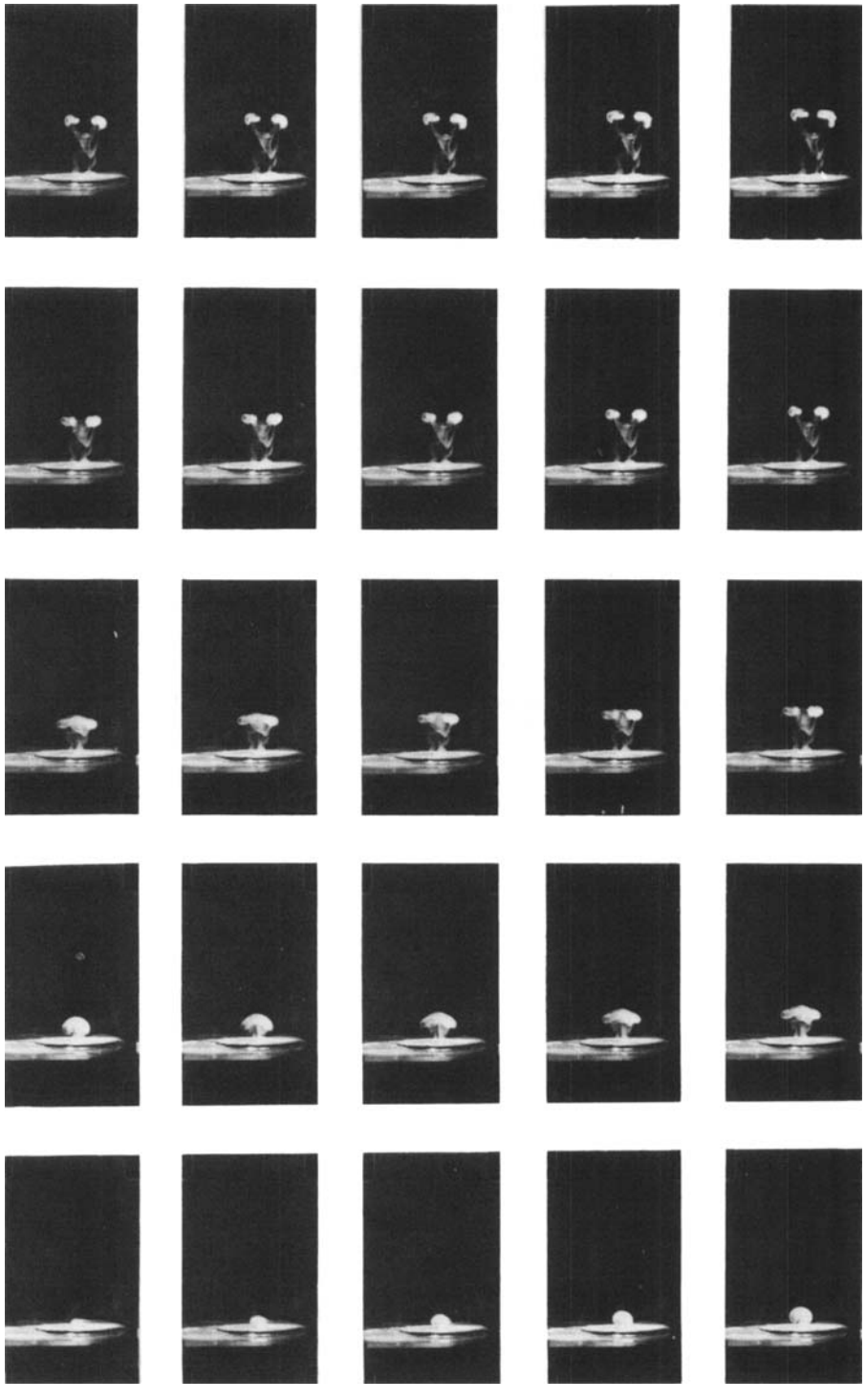

FIGURE 14. Side-view of the break-up process of the vortex ring in the case $b/a = 0{\cdot}2$. The order of the sequence is as in figure 11. The film sequence was taken at 32 frames/s.

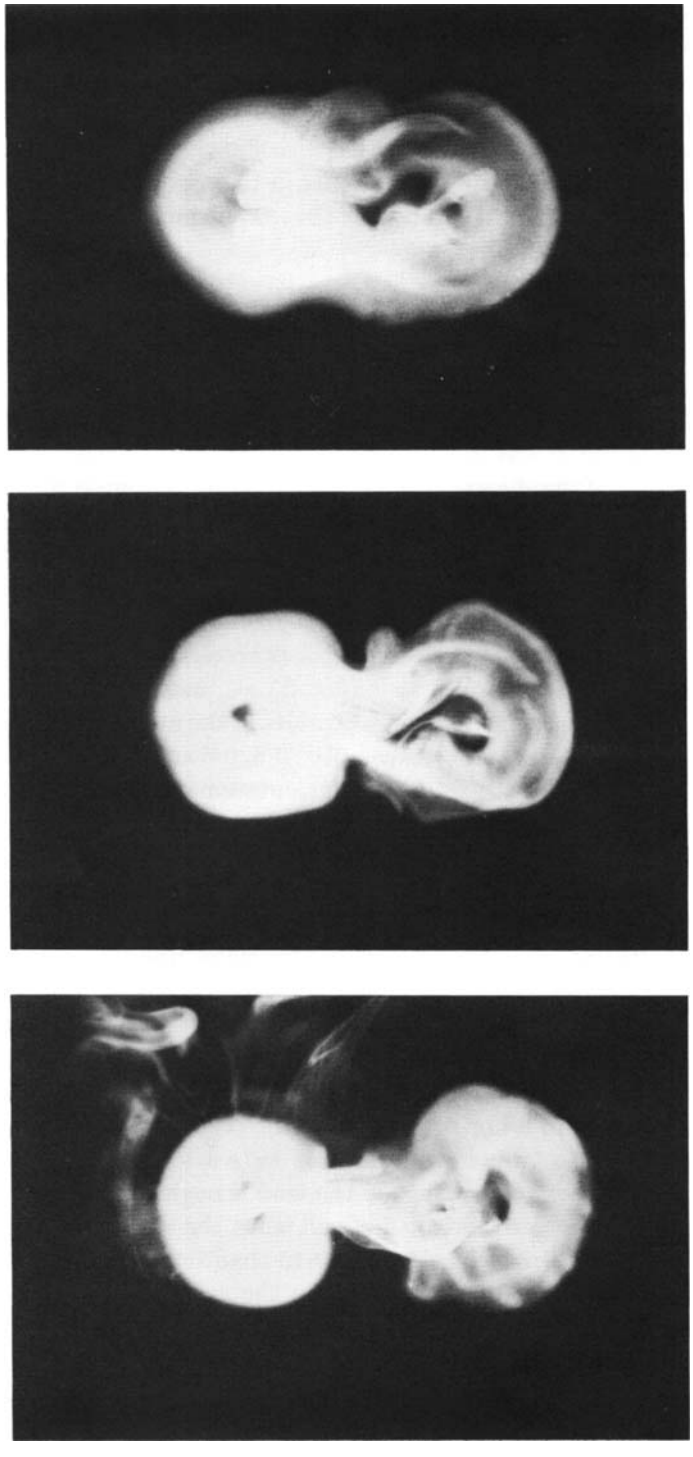

FIGURE 15. Detailed plan view of the break-up of the vortex ring in the case $b/a = 0{\cdot}2$.

angles is such that the vortex rings move almost parallel to each other. At the Reynold's number of the experiment, the rings were not observed to rejoin. In figure 15 individual photographs of the plan view of the vortex ring at different stages of the break-up process are shown.† The time of the break-up of the vortex ring is shown in figure 10; the time of the break-up anticipated in §4 is also shown in the figure. It may be noted that a break-up of the vortex ring also occurs in the case of a ring produced from an orifice in the form of a narrow rectangular slit (see Kambe & Takao (1971)); the ring breaks up into three smaller rings.

7. Discussion

By means of numerical calculations using the cut-off approximation, it has been shown that a flat elliptic vortex ring of axes ratio, 0·8, 0·6 and 0·4 oscillates in time, the oscillations being periodic only in the first of these cases. At the end of a half oscillation cycle, the deviations of the shape of the vortex ring from an ellipse with the orientation of its axes reversed becomes more pronounced as more eccentric cases are considered. In the case of a ring of axes ratio 0·2, it is anticipated in §4 that the vortex ring would break-up through the touching of the cores of distinct portions of the vortex ring. This suggests that there is a critical axes ratio, $(b/a)_{cr}$, $0{\cdot}4 > (b/a)_{cr} \geqslant 0{\cdot}2$, above which an elliptic vortex ring oscillates and below which it breaks up.

The results from experiments conducted at moderate Reynold's number ($\Gamma/\nu \sim 2000$) are in fair agreement with the results of the numerical computations. The vortex ring oscillates in the cases of axes ratios 0·8, 0·6 and 0·4 in a manner strikingly similar to that anticipated by the numerical calculations. In the case of the vortex ring of axes ratio 0·2, the vortex ring breaks up into two smaller rings; however, the break-up only occurs when the Reynold's number is high enough ($\Gamma/\nu > 1300$ approximately).

The vortex trail of an aircraft breaks up into vortex rings as can be seen from the photograph (figure 1) in Crow's (1970) paper. The photograph shows that in the plane of maximum area (the horizontal plane) the vortex rings, when they form, have roughly elliptic shape.

Using, as approximations, the data from Crow's paper ($\Gamma = 268$ m^2 s^{-1}, so that $\Gamma/\nu = 1{\cdot}8 \times 10^7$, core radius $c_0 = 2{\cdot}7$ m for a B-47 aircraft of span 35 m and moving at 220 m s^{-1}), and assuming that each ring when formed has an elliptic shape with axes ratio 0·2, is flat and lies in a horizontal plane, the results of §§4–6 suggest that each ring would break up into two smaller rings at 107 s after the initial ring formation; here the influence of other vortex rings in the trail is neglected. Since a vortex ring in an aircraft trail, when formed, is not flat and since the axes ratio appears from the photograph in Crow's paper to be closer to 0·15 than 0·2 (also the size of the core is comparatively much smaller than that used in the calculations and observed in the experiments) it is expected that the actual break up of the vortex ring would occur at an earlier time.

Not enough information is available in the photograph. However, on comparison with figure 5, it appears that the break-up may occur 30–40 s after the initial ring formation.

† The photographs in figure 15 may be compared with figure 8 of Oshima & Asaka (1977*a*) which show the 'reverse' process in which two small circular vortex rings combine to form one large ring of roughly elliptic shape.

We are grateful to Professor D. W. Moore for suggesting the problem to us. One of us (M. R. D.) is indebted to him for his encouragement and guidance during the course of research work, part of which formed the basis of this paper. During the preparation of this paper M. R. D. was financially supported by the Science Research Council.

Appendix A. Initial core size used in the numerical calculations

A process of generation of a vortex ring in a perfect fluid by an impulsive motion and subsequent annihilation of a flat elliptic disk is considered here (cf. G. I. Taylor 1953).

Suppose in Cartesian co-ordinate system, the edge of the disk is given by

$$\frac{x^2}{a_0^2}+\frac{y^2}{b_0^2}=1 \quad (a_0 > b_0). \tag{A 1}$$

Then if the disk is moved impulsively from rest at speed U normal to its plane, the velocity potential at the disk is given by

$$\phi = \mp \frac{Ub_0}{E(e)}\left(1-\frac{x^2}{a_0^2}-\frac{y^2}{b_0^2}\right)^{\frac{1}{2}}, \tag{A 2}$$

where

$$e^2=\frac{(a_0^2-b_0^2)}{a_0^2}, \quad E(e)=\int_0^{\frac{1}{2}\pi}(1-e^2\sin^2\theta)^{\frac{1}{2}}\,d\theta,$$

are respectively the eccentricity of the ellipse and elliptic integral of the second kind. The kinetic energy of the flow is given by

$$\begin{aligned} T_D &= -\frac{1}{2}\iint \phi \frac{\partial\phi}{\partial n}\,dS \\ &= \frac{2\pi a_0 b_0^2 U^2}{3E(e)}, \end{aligned} \tag{A 3}$$

and the impulse is given by

$$\begin{aligned} I_D &= \frac{dT_D}{dU} \\ &= \frac{4\pi a_0 b_0^2 U}{3E(e)}, \end{aligned} \tag{A 4}$$

If now the disk is dissolved away, a finite vortex sheet is left behind, the vortex lines being ellipses of the same axes ratio as the disk. Writing $x = cr_e\cos\theta$, $y = dr_e\sin\theta$ $(0 \leqslant r_e \leqslant 1,\ -\pi \leqslant \theta \leqslant \pi)$, the circulation of the portion $(r_e, 1)$ for any fixed θ is, from (A 2),

$$\frac{2Ub_0}{E(e)}(1-r_e^2)^{\frac{1}{2}}. \tag{A 5}$$

This configuration cannot persist because the self-induced velocity is infinite at $r_e = 1$. The vortex elements respond in such a way that the stronger vortex lines near $r_e = 1$ tend to roll up the weaker parts near $r_e = 0$ round them. Thus the vorticity tends to concentrate in an elliptic ring of major axis a and minor axis b, say, and of circulation Γ given by

$$\Gamma = \frac{2Ub_0}{E(e)}. \tag{A 6}$$

The impulse I and kinetic energy T of a vortex filament are given by Moore & Saffman (1972) as

$$T = \frac{\Gamma}{2}\oint \mathbf{X} \wedge \hat{\mathbf{t}}\, ds$$

$$T = \oint \left\{\frac{\Gamma^2}{4\pi}\left[\ln\frac{8\rho}{c_0} - 2 + A + \frac{\hat{\mathbf{t}}.\mathbf{X}}{\rho}\frac{\partial\rho}{\partial s}\right] - \Gamma(\mathbf{X}\wedge\mathbf{V}_1.\hat{\mathbf{t}})\right\} ds$$

where $\rho(s)$ is the radius of curvature, $\mathbf{X}$ is as in (3.1) and $\mathbf{V}_1$ is approximately given by the right-hand side of (3.1) less a velocity of a circular vortex ring of radius ρ and lying along the osculating circle at $\mathbf{X}$. For an elliptic vortex ring, therefore

$$\mathbf{I} \equiv \mathbf{I}_R = \Gamma\pi ab\mathbf{k} \tag{A 7}$$

and

$$T \equiv T_R = \frac{\Gamma^2 a}{\pi}\left[\left(\ln\left(\frac{8(ab)^{\frac{1}{2}}}{c_0}\right) - 1 + A\right)E(e) - (1-\tfrac{1}{2}e^2)\,K(e)\right] \tag{A 8}$$

where $K(e)$ is the elliptic integral of the first kind.

Following Taylor (1953), it may be assumed that

$$T_D = T_R, \quad I_D = I_R \tag{A 9}$$

so that using (A 6), we have

$$ab = \tfrac{2}{3}a_0 b_0 \tag{A 10}$$

and core radius c_0 is

$$c_0 = 8(ab)^{\frac{1}{2}}\exp\left[-\frac{\pi^2}{2\sqrt{6}} - 1 + A - (1-\tfrac{1}{2}e^2)\frac{K(e)}{E(e)}\right]. \tag{A 11}$$

Appendix B. Estimate of vortex parameters using Saffman's (1978) model

Estimates of the circulation Γ, the core radius $c_0 (\equiv C_E)$ and the size of the elliptic vortex ring generated can be obtained in the manner suggested by Saffman (1978) for circular vortex rings. Here it is assumed that when the flow has just been set into motion, and the vortex sheet is of small extent and close to the edge, it behaves like a two-dimensional vortex sheet formed at the edge of a semi-infinite flat plate lying along $z = 0, n > 0$ (see figure 16*a*, *b*). Initially the velocity potential is given by

$$\phi = -\alpha r^{\frac{1}{2}}\cos\tfrac{1}{2}\chi \tag{B 1}$$

where $r = (n^2+z^2)^{\frac{1}{2}}$ and α is determined by matching to the flow far from the edge. For flow through an elliptic orifice of semi-major axis a_0 and semi-minor axis b_0 in an infinite plane, the normal velocity V_z at the orifice is given by Lamb (1932, p. 151). Near a point (x_0, y_0) on the edge of the ellipse, this is approximately

$$\frac{\sqrt{2}\,A\,|n|^{-\frac{1}{2}}}{a_0 b_0^{\frac{1}{2}}(1-e^2\cos^2\theta_0)^{\frac{1}{4}}}$$

where $4\pi A$ is the flux through the hole and e is the eccentricity of the ellipse. By comparing this with

$$\frac{1}{r}\frac{\partial\phi}{\partial\chi}\bigg|_{\substack{\chi=\pi\\ r=|n|}},$$

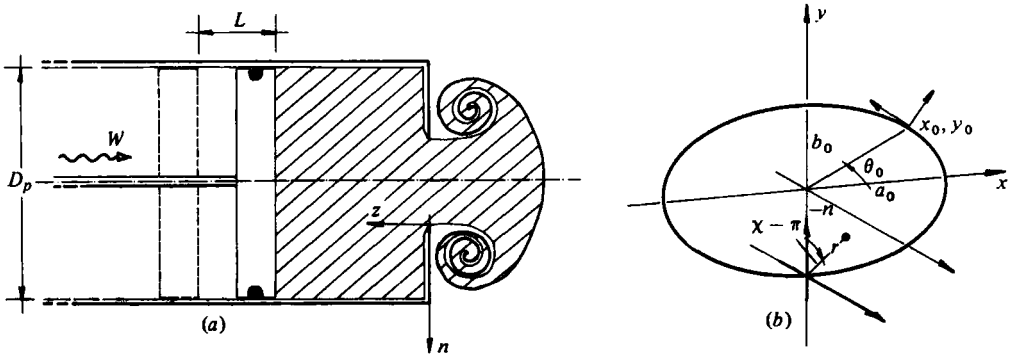

FIGURE 16.

an estimate of α can be obtained. However, α varies along the edge of the orifice which is undesirable. Thus an average value is taken

$$\alpha = 2|n|^{\frac{1}{2}} \left(\frac{\int_0^{\frac{1}{2}\pi} V_z^2 \left| \frac{ds}{d\theta} \right| d\theta}{\int_0^{\frac{1}{2}\pi} \left| \frac{ds}{d\theta} \right| d\theta} \right)^{\frac{1}{2}} = \frac{2\sqrt{\pi A}}{a_0 b_0^{\frac{1}{2}} E^{\frac{1}{2}}(e)}. \tag{B 2}$$

Then for small times, the vortex sheet which appears at the edge depends on α and t only. Its centre (N_1, Z_1), circulation $\Gamma(r_1)$ about a small circle centred on the vertex of the spiral and total circulation Γ shed from the edge is given by

$$\left.\begin{aligned} N_1 = c_1(\alpha t)^{\frac{3}{2}}, \quad Z_1 = c_2(\alpha t)^{\frac{3}{2}}, \quad \Gamma(r_1) = c_3 \alpha r_1^{\frac{1}{2}}, \\ \Gamma = c_4 \alpha^{\frac{3}{2}} t^{\frac{1}{2}}, \end{aligned}\right\} \tag{B 3}$$

where c_1, c_2, c_3 and c_4 are constants (estimates obtained from Pullin's (1978) calculations are $c_1 = 0{\cdot}08$, $c_2 = 0{\cdot}34$, $c_3 = 4{\cdot}08$, $c_4 = 2{\cdot}40$).

If the piston stops moving at time $t = W/L$ where W is the velocity of the piston and L is the displacement, the rolled-up vortex sheet breaks away from the edge of the orifice. The semi-axes, a and b, core radius C_E and circulation Γ of the ensuing vortex ring are then given by

$$\left.\begin{aligned} a = a_0 + c_1 \left(\frac{\alpha L}{W}\right)^{\frac{3}{2}}, \quad b = b_0 + c_1 \left(\frac{\alpha L}{W}\right)^{\frac{3}{2}}, \\ c_0 = \frac{c_4^2}{c_3^2} \left(\frac{\alpha L}{W}\right)^{\frac{3}{2}}, \quad \Gamma = c_4 \alpha^{\frac{3}{2}} \left(\frac{L}{W}\right)^{\frac{3}{2}}. \end{aligned}\right\} \tag{B 4}$$

Since $a/b \neq a_0/b_0$, the vortex ring will have a different eccentricity from that of the orifice. However, for small values of L this change will be small. Also, the interaction of the ring with the wall would lead to a decrease in a and b below that given in (B 4) (Sheffield 1977). Hence, for the range of eccentricities used here, this discrepancy is ignored and a and b are taken to be

$$a = a_0 \left[1 + \frac{c_1(a_0 + b_0)}{2a_0 b_0} \left(\frac{\alpha L}{W}\right)^{\frac{3}{2}} \right], \quad b = b_0 \left[1 + \frac{c_1(a_0 + b_0)}{2a_0 b_0} \left(\frac{\alpha L}{W}\right)^{\frac{3}{2}} \right]. \tag{B 5}$$

From (B 1) the swirl velocity in the core is $\sim r^{-\frac{1}{2}}$.

REFERENCES

ARMS, R. J. & HAMA, F. R. 1965 Localized-induction concept on a curved vortex and motion of an elliptic vortex ring. *Phys. Fluids.* **8**, 553.

CROW, S. C. 1970 Stability theory for a pair of trailing vortices. *A.I.A.A. J.* **8**, 2172.

DIDDEN, N. 1979 On the formation of vortex rings. *Z. angew. Math. Phys.* **30**, 101.

FOHL, T. & TURNER, J. S. 1975 Colliding vortex rings. *Phys. Fluids* **18**, 433.

FRAENKEL, L. E. 1970 On steady vortex rings of small cross-section in an ideal fluid. *Proc. Roy. Soc.* A **316**, 29.

KAMBE, T. & TAKAO, T. 1971 Motion of distorted vortex rings. *J. Phys. Soc. Japan* **31**, 591.

KOKSHAYSKY, N. V. 1979 Tracing the wake of a flying bird. *Nature* **279**, 176.

LAMB, H. 1932 *Hydrodynamics.* Dover.

LEONARD, A. 1974 Numerical simulation of interacting three-dimensional vortex filaments. *Proc. 4th Int. Conf. Numerical Methods in Fluid Dynamics*, p. 245. Springer.

MOORE, D. W. 1972 Finite amplitude waves on aircraft trailing vortices. *Aeronaut. Quart.* **23**, 307.

MOORE, D. W. & SAFFMAN, P. G. 1972 The motion of a vortex filament with axial flow. *Phil. Trans. R. Soc.* A **272**, 403.

NORBURY, J. 1978 A family of steady vortex rings. *J. Fluid Mech.* **57**, 417.

OSHIMA, Y. 1972 Motion of vortex rings in water. *J. Phys. Soc. Japan* **32**, 1125.

OSHIMA, Y. 1978 Head-on collision of two vortex rings. *J. Phys. Soc. Japan* **44**, 328.

OSHIMA, Y. & ASAKA, S. 1977*a* Interaction of two vortex rings along parallel axes in air, *J. Phys. Soc. Japan* **42**, 708.

OSHIMA, Y. & ASAKA, S. 1977*b* Interaction of multi-vortex rings, *J. Phys. Soc. Japan* **42**, 1391.

PULLIN, D. I. 1978 The large-scale structure of unsteady self-similar rolled-up vortex sheets. *J. Fluid Mech.* **88**, 401.

RAYNER, J. M. V. 1979 A vortex theory of animal flight. Part 2. The forward flight of birds. *J. Fluid Mech.* **91**, 731.

SAFFMAN, P. G. 1970 The velocity of viscous vortex rings. *Stud. Appl. Math.* **49**, 371.

SAFFMAN, P. G. 1978 The number of waves on unstable vortex rings. *J. Fluid Mech.* **84**, 625.

SALLET, D. W. 1975 Impulsive motion of a circular disk which causes a vortex ring. *Phys. Fluids* **18**, 109.

SALLET, D. W. & WIDEMAYER, R. S. 1974 An experimental investigation of laminar and turbulent vortex rings in air. *Z. Flugwiss.* **22**, 207.

SHEFFIELD, J. S. 1977 Trajectories of an ideal vortex pair near an orifice. *Phys. Fluids* **20**, 543.

TAYLOR, G. I. 1953 Formation of a vortex ring by giving an impulse to a circular disc and then dissolving it away. *J. Appl. Phys.* **24**, 104.

VIETS, H. & SFORZA, P. M. 1975 Dynamics of bilaterally summetric vortex rings. *Phys. Fluids* **15**, 230.

WIDNALL, S. E., BLISS, D. B. & ZALAY, A. 1971 Theoretical and experimental study of the stability of a vortex pair. In *Aircraft Wake Turbulence and its Detection* (ed. J. H. Olsen, A. Goldburg & M. Rogers), pp. 305–338. Plenum.

WIDNALL, S. E. & SULLIVAN, J. P. 1973 On the stability of vortex rings. *Proc. R. Soc.* A **322**, 335.

WIDNALL, S. E. & TSAI, C. Y. 1977 The instability of a thin vortex ring of constant vorticity. *Phil. Trans. R. Soc.* A **287**, 273.